GEOPHYSICS, VOL. 85, NO. 2 (MARCH-APRIL 2020); P. A1–A5, 7 FIGS.
10.1190/GEO2019-0407.1

Discrete representations for Marchenko imaging of imperfectly sampled data

Kees Wapenaar[1] and Johno van IJsseldijk[1]

ABSTRACT

Marchenko imaging is based on integral representations for focusing functions and Green's functions. In practice, the integrals are replaced by finite summations. This works well for regularly sampled data, but the quality of the results degrades in a case of imperfect sampling. We have developed discrete representations that account for imperfect sampling of the sources (or, via reciprocity, of the receivers). These representations contain point-spread functions that explain the blurring of the focusing functions and Green's functions due to imperfect sampling. Deblurring the focusing functions and Green's functions involves multidimensional deconvolution for the point-spread functions. The discrete representations form the basis for modifying Marchenko imaging to account for imperfectly sampled data, which is important for field data applications.

INTRODUCTION

Marchenko imaging is based on integral representations for Green's functions with virtual sources and/or receivers in the subsurface (Broggini and Snieder, 2012; Slob et al., 2014; Wapenaar et al., 2014). In practice, the integrals are replaced by finite summations over the available sources (or, via reciprocity, over the available receivers). This works well for regularly sampled sources (or receivers) obeying the Nyquist criterion, on a large enough grid. Most authors who use the Marchenko method tacitly assume that these conditions are fulfilled; however, some authors have investigated the effects of imperfect sampling. Peng et al. (2019) numerically evaluate the effects of downsampling the sources and/or receivers in a regular way. Staring and Wapenaar (2019) numerically investigate the effects of missing near offsets, limited crossline aperture, and undersampling in the crossline direction on 3D Marchenko imaging. Apart from evaluating the effects of imperfect sampling, one would also like to compensate for them. Ravasi (2017) and Haindl et al. (2018) consider the situation of irregularly sampled sources and well-sampled receivers. Using reciprocity, they reformulate the representation integrals along the well-sampled receivers and propose a sparse inversion method to compensate for the source irregularity.

Ultimately, one would like to compensate for imperfect sampling of the sources as well as the receivers. This paper makes a first step in that direction by reformulating the integral representations in terms of discrete finite summations over imperfectly sampled sources. This is akin to reformulating the representations underlying seismic interferometry for irregular source distributions. For seismic interferometry, the approach is as follows. The classic correlation integral representation is replaced by an implicit convolution integral representation, which is subsequently inverted by multidimensional deconvolution (MDD) (Wapenaar et al., 2011). The point-spread function (PSF) plays a central role in this approach (Van der Neut and Wapenaar, 2015). This approach is not straightforwardly adapted for Marchenko imaging because this method is based on a combination of convolution and correlation integral representations. Following a different route, we derive discrete representations for Marchenko imaging, which include PSFs. We illustrate these representations with numerical examples. These representations form the basis for modified Marchenko imaging of imperfectly sampled data, which is the subject of ongoing research.

INTEGRAL REPRESENTATIONS

We consider an inhomogeneous lossless acoustic medium bounded by acquisition surface $\mathbb{S}_0$ (Figure 1a). We assume that this surface is reflection free and that the half-space above it is homogeneous. The reflection response at this surface is given by $R(\mathbf{x}_R, \mathbf{x}_S, t)$, where $\mathbf{x}_S$ and $\mathbf{x}_R$ denote the source and receiver positions, respectively, and t

Manuscript received by the Editor 26 June 2019; revised manuscript received 9 October 2019; published ahead of production 19 November 2019; published online 30 January 2020.
[1]Delft University of Technology, Department of Geoscience and Engineering, Delft, The Netherlands. E-mail: c.p.a.wapenaar@tudelft.nl (corresponding author); j.e.vanijsseldijk@tudelft.nl.

denotes the time. Let us define a virtual receiver position $\mathbf{x}_A$ inside the inhomogeneous medium. The Green's functions from the surface $\mathbb{S}_0$ to this virtual receiver are given by $G^+(\mathbf{x}_A, \mathbf{x}_R, t)$ and $G^-(\mathbf{x}_A, \mathbf{x}_R, t)$, where the superscripts $+$ and $-$ denote downward and upward propagation, respectively, at $\mathbf{x}_A$. Next, we define a horizontal surface $\mathbb{S}_A$ at the depth of the virtual receiver. We consider a truncated version of the medium, which is identical to the actual medium above $\mathbb{S}_A$ and homogeneous below it (Figure 1b). At $\mathbb{S}_0$ we introduce a downgoing focusing function $f_1^+(\mathbf{x}_S, \mathbf{x}_A, t)$ that, when emitted from all $\mathbf{x}_S$ at $\mathbb{S}_0$ into the truncated medium, focuses at $\mathbf{x}_A$. Its upgoing response at $\mathbb{S}_0$ is denoted by $f_1^-(\mathbf{x}_R, \mathbf{x}_A, t)$.

All of these quantities are related via the following integral representations:

$$G^-(\mathbf{x}_A, \mathbf{x}_R, t) + f_1^-(\mathbf{x}_R, \mathbf{x}_A, t) = \int_{\mathbb{S}_0} R(\mathbf{x}_R, \mathbf{x}_S, t) * f_1^+(\mathbf{x}_S, \mathbf{x}_A, t) \mathrm{d}\mathbf{x}_S, \tag{1}$$

$$G^+(\mathbf{x}_A, \mathbf{x}_R, t) - f_1^+(\mathbf{x}_R, \mathbf{x}_A, -t) = -\int_{\mathbb{S}_0} R(\mathbf{x}_R, \mathbf{x}_S, t) * f_1^-(\mathbf{x}_S, \mathbf{x}_A, -t) \mathrm{d}\mathbf{x}_S, \tag{2}$$

where the asterisk $(*)$ denotes the temporal convolution. These representations hold for flux-normalized as well as pressure-normalized wavefields (Wapenaar et al., 2014).

We illustrate these representations with a 2D numerical example, assuming for the moment that the source positions $\mathbf{x}_S$ are regularly distributed along $\mathbb{S}_0$. For simplicity, we consider a horizontally layered medium, of which the propagation velocity and mass density as a function of depth are shown in Figure 2. We define $\mathbb{S}_0$ at $x_3 = 0$ m and $\mathbb{S}_A$ at $x_3 = 1000$ m. We numerically model the reflection response at $\mathbb{S}_0$ and convolve it with a Ricker wavelet with a central frequency of 25 Hz. Also, the focusing functions are numerically modeled (because the aim of this paper is to investigate representations rather than the performance of the Marchenko method). We evaluate the integrals in the right sides of equations 1 and 2 for a fixed receiver position ($x_{1,R} = 0$), using regular source sampling ($\Delta x_{1,S} = 5$ m, and the number of sources is 601). The results are shown in Figure 3a and 3b, respectively. The dashed red lines separate the retrieved focusing functions from the Green's functions at the left sides of equations 1 and 2 (except for the first event below the red line in Figure 3b, which belongs to the focusing function and the Green's function, as indicated by the arrows).

In practice, the right sides of equations 1 and 2 are approximated by summations, according to

$$\sum_i R(\mathbf{x}_R, \mathbf{x}_S^{(i)}, t) * f_1^+(\mathbf{x}_S^{(i)}, \mathbf{x}_A, t) * S(t) \tag{3}$$

and

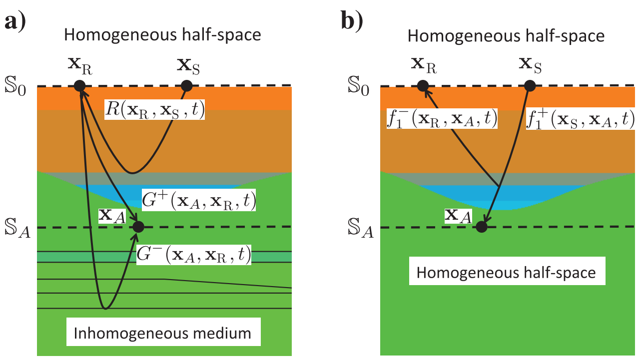

Figure 1. (a) Inhomogeneous medium, its reflection response, and Green's functions. (b) Truncated medium with focusing functions. In both figures, the rays stand for full responses, including all orders of multiple scattering.

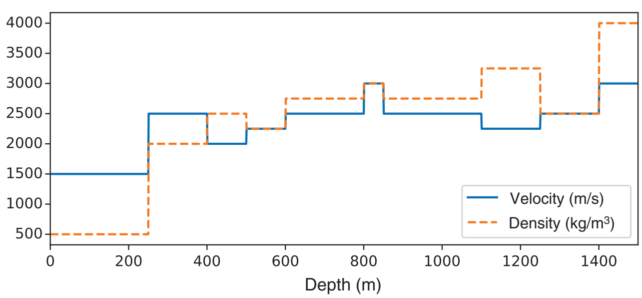

Figure 2. Propagation velocity and mass density of a horizontally layered medium as a function of depth.

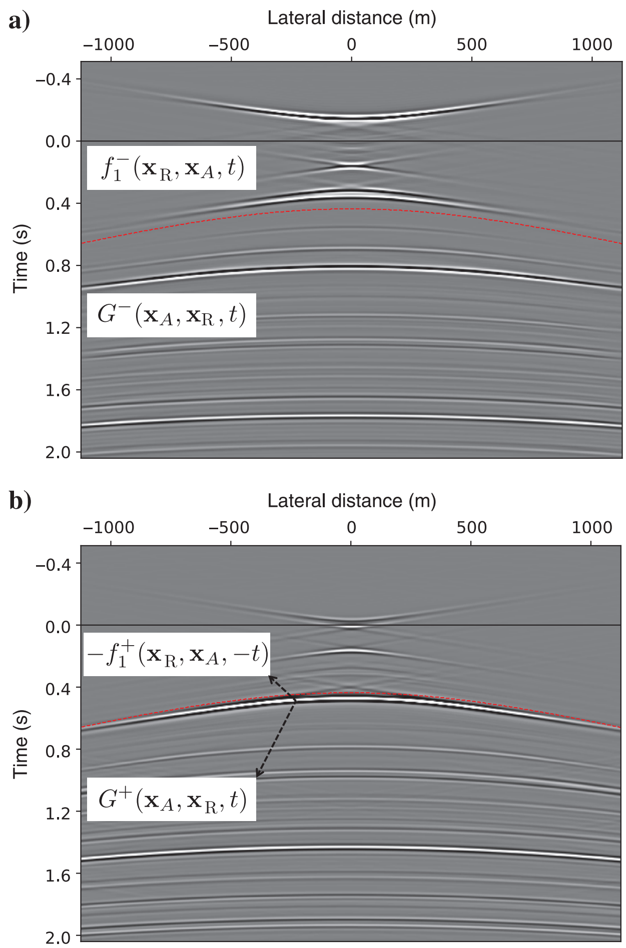

Figure 3. Evaluation of the integrals in equations 1 and 2, for fixed $\mathbf{x}_R$ at $\mathbb{S}_0$ and variable $\mathbf{x}_A$ along $\mathbb{S}_A$.

$$-\sum_i R(\mathbf{x}_R, \mathbf{x}_S^{(i)}, t) * f_1^-(\mathbf{x}_S^{(i)}, \mathbf{x}_A, -t) * S(t), \qquad (4)$$

respectively, with $S(t)$ being the source wavelet. Assuming that the source position $\mathbf{x}_S^{(i)}$ is imperfectly sampled, these approximations have an effect on the retrieved focusing functions and Green's functions. We illustrate this with a numerical example. Figure 4 shows an irregular distribution of source positions $\mathbf{x}_S^{(i)}$ along $\mathbb{S}_0$ (the average $\Delta x_{1,S} = 16.7$ m, and the number of sources is 181). We evaluate equations 3 and 4, using resampled versions of the reflection response and focusing functions of the previous example (the sources are resampled; the receiver position is again fixed at $x_{1,R} = 0$). The results, which are shown in Figure 5a and 5b, respectively, are blurred versions of those in Figure 3. This blurring can be quantified by PSFs, which are introduced in the next section.

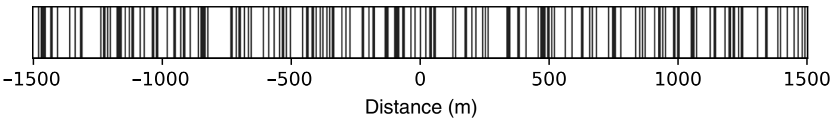

Figure 4. Irregular distribution of $\mathbf{x}_S^{(i)}$ along $\mathbb{S}_0$. The black bars denote the positions of the sources.

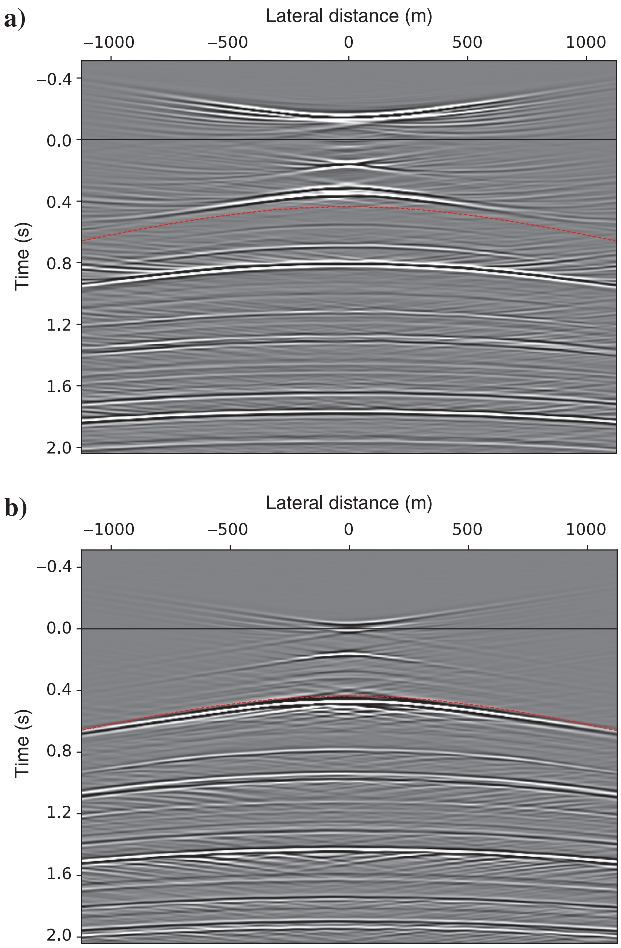

Figure 5. Evaluation of the irregular summations in equations 3 and 4, for fixed $\mathbf{x}_R$ at $\mathbb{S}_0$ and variable $\mathbf{x}_A$ along $\mathbb{S}_A$.

POINT-SPREAD FUNCTIONS

The focusing function f_1^+ is defined as the inverse of the transmission response between $\mathbb{S}_0$ and $\mathbb{S}_A$. This is quantified as follows:

$$\delta(\mathbf{x}'_{H,A} - \mathbf{x}_{H,A})\delta(t) = \int_{\mathbb{S}_0} T(\mathbf{x}'_A, \mathbf{x}_S, t) * f_1^+(\mathbf{x}_S, \mathbf{x}_A, t)\mathrm{d}\mathbf{x}_S, \qquad (5)$$

with $\mathbf{x}'_A$ and $\mathbf{x}_A$ at $\mathbb{S}_A$, and $\mathbf{x}'_{H,A}$ and $\mathbf{x}_{H,A}$ denote the horizontal coordinates of $\mathbf{x}'_A$ and $\mathbf{x}_A$, respectively. Here, T stands for the flux-normalized transmission response or for a modified version $\mathcal{T}$ of the pressure-normalized transmission response (Wapenaar et al., 2014). For the case of imperfect sampling, the discretized band-limited version of equation 5 reads

$$\Gamma^+(\mathbf{x}'_A, \mathbf{x}_A, t) = \sum_i T(\mathbf{x}'_A, \mathbf{x}_S^{(i)}, t) * f_1^+(\mathbf{x}_S^{(i)}, \mathbf{x}_A, t) * S(t), \qquad (6)$$

where $\Gamma^+(\mathbf{x}'_A, \mathbf{x}_A, t)$ is a PSF. It is illustrated in Figure 6a (obtained from the numerically modeled f_1^+ and T), for the same irregular source distribution that was used in the example in Figure 5. In the next section, we show that this PSF explains the blurring in Figure 5a. However, it does not explain the blurring in Figure 5b. For this we need a second PSF, which we discuss now.

Analogous to equation 5, we define a quantity Y as the inverse of f_1^- as follows:

$$\delta(\mathbf{x}'_{H,A} - \mathbf{x}_{H,A})\delta(t) = \int_{\mathbb{S}_0} Y(\mathbf{x}'_A, \mathbf{x}_S, t) * f_1^-(\mathbf{x}_S, \mathbf{x}_A, -t)\mathrm{d}\mathbf{x}_S. \qquad (7)$$

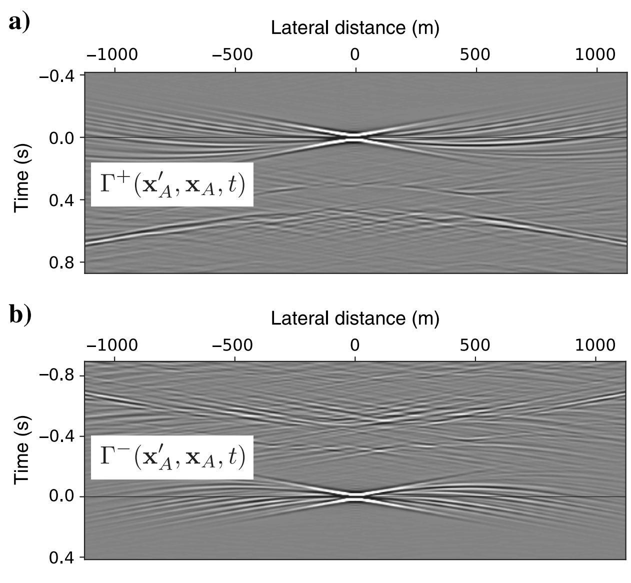

Figure 6. The PSFs, as defined in equations 6 and 8, for fixed $\mathbf{x}'_A$ and variable $\mathbf{x}_A$, at $\mathbb{S}_A$. These PSFs quantify the blurring in Figure 5a and 5b, respectively.

In the following, we tacitly assume that Y exists, but we remark that because f_1^- is a reflection response, inversion of equation 7 for Y may not always be stable. Analogous to equation 6, we define a PSF for the case of imperfect sampling as follows:

$$\Gamma^-(\mathbf{x}'_A, \mathbf{x}_A, t) = \sum_i Y(\mathbf{x}'_A, \mathbf{x}_S^{(i)}, t) * f_1^-(\mathbf{x}_S^{(i)}, \mathbf{x}_A, -t) * S(t), \tag{8}$$

which is illustrated in Figure 6b (obtained from the numerically modeled f_1^- and Y).

DISCRETE REPRESENTATIONS

We use the PSFs introduced in the previous section to transform the integral representations of equations 1 and 2 into discrete representations. We start by applying the operation $\int_{\mathbb{S}_A}\{\cdot\} * \Gamma^+(\mathbf{x}'_A, \mathbf{x}_A, t)\mathrm{d}\mathbf{x}'_A$ to both sides of equation 1 (with $\mathbf{x}_A$ replaced by $\mathbf{x}'_A$). For the terms on the left side, we define the blurred functions $\hat{G}^-$ and $\hat{f}_1^-$, according to

$$\hat{G}^-(\mathbf{x}_A, \mathbf{x}_R, t) = \int_{\mathbb{S}_A} G^-(\mathbf{x}'_A, \mathbf{x}_R, t) * \Gamma^+(\mathbf{x}'_A, \mathbf{x}_A, t)\mathrm{d}\mathbf{x}'_A, \tag{9}$$

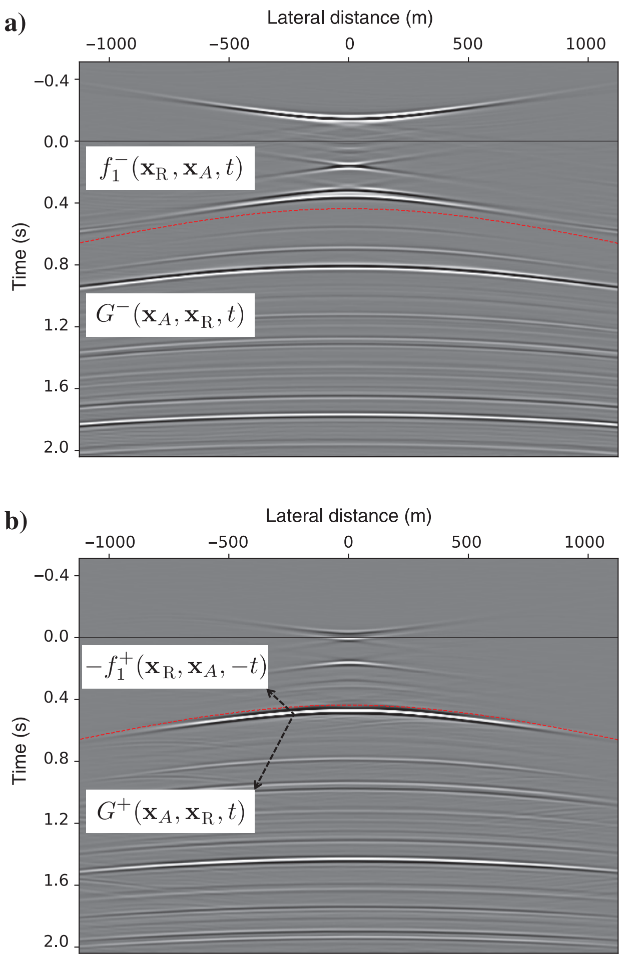

Figure 7. Results of deblurring Figure 5a and 5b by MDD.

$$\hat{f}_1^-(\mathbf{x}_R, \mathbf{x}_A, t) = \int_{\mathbb{S}_A} f_1^-(\mathbf{x}_R, \mathbf{x}'_A, t) * \Gamma^+(\mathbf{x}'_A, \mathbf{x}_A, t)\mathrm{d}\mathbf{x}'_A. \tag{10}$$

Applying the same operation to the right side of equation 1, substituting equation 6 and interchanging the order of summation over $\mathbf{x}_S^{(i)}$ and integration along $\mathbb{S}_A$, we obtain

$$\sum_i \int_{\mathbb{S}_0} R(\mathbf{x}_R, \mathbf{x}_S, t) * f_1^+(\mathbf{x}_S^{(i)}, \mathbf{x}_A, t) * S(t) * \int_{\mathbb{S}_A} f_1^+(\mathbf{x}_S, \mathbf{x}'_A, t) * T(\mathbf{x}'_A, \mathbf{x}_S^{(i)}, t)\mathrm{d}\mathbf{x}'_A\mathrm{d}\mathbf{x}_S. \tag{11}$$

Because T and f_1^+ are each other's inverse, the integral along $\mathbb{S}_A$ yields $\delta(\mathbf{x}_{H,S} - \mathbf{x}_{H,S}^{(i)})\delta(t)$, where $\mathbf{x}_{H,S}$ and $\mathbf{x}_{H,S}^{(i)}$ denote the horizontal coordinates of $\mathbf{x}_S$ and $\mathbf{x}_S^{(i)}$, respectively. Using the sift property of this delta function in the integral along $\mathbb{S}_0$, what remains of equation 11 is a summation over $\mathbf{x}_S^{(i)}$, precisely as formulated in equation 3. Combining the results, we thus obtain

$$\hat{G}^-(\mathbf{x}_A, \mathbf{x}_R, t) + \hat{f}_1^-(\mathbf{x}_R, \mathbf{x}_A, t) = \sum_i R(\mathbf{x}_R, \mathbf{x}_S^{(i)}, t) * f_1^+(\mathbf{x}_S^{(i)}, \mathbf{x}_A, t) * S(t). \tag{12}$$

This discrete representation is the counterpart of the integral representation of equation 1. The right side can be seen as the practical implementation of the integral in equation 1 when the sources $\mathbf{x}_S^{(i)}$ are imperfectly sampled. The left side contains blurred versions of the Green's function and the focusing function. According to equation 9, the receiver of the Green's function is smeared around $\mathbf{x}_A$ by the PSF $\Gamma^+(\mathbf{x}'_A, \mathbf{x}_A, t)$. Similarly, equation 10 quantifies the smearing by the PSF of the focal point of the focusing function around $\mathbf{x}_A$. Hence, the PSF $\Gamma^+(\mathbf{x}'_A, \mathbf{x}_A, t)$ explains the blurring observed in Figure 5a. We deblur this figure by MDD, that is, by applying the least-squares inverse of the PSF to $\hat{G}^-(\mathbf{x}_A, \mathbf{x}_R, t) + \hat{f}_1^-(\mathbf{x}_R, \mathbf{x}_A, t)$ (for fixed $\mathbf{x}_R$ and variable $\mathbf{x}_A$). Note that, although the medium is laterally invariant, the PSF is not shift-invariant due to the irregular sampling. Hence, MDD requires a full matrix inversion. The result is shown in Figure 7a and accurately matches the ideal result in Figure 3a. The maximum deviation for the central trace is 2.4%. At far offsets, the amplitudes are somewhat overestimated due to limitations of the MDD method.

Next, we apply the operation $\int_{\mathbb{S}_A}\{\cdot\} * \Gamma^-(\mathbf{x}'_A, \mathbf{x}_A, t)\mathrm{d}\mathbf{x}'_A$ to both sides of equation 2 (with $\mathbf{x}_A$ replaced by $\mathbf{x}'_A$). In a similar way as above, we obtain

$$\hat{G}^+(\mathbf{x}_A, \mathbf{x}_R, t) - \hat{f}_1^+(\mathbf{x}_R, \mathbf{x}_A, -t) = -\sum_i R(\mathbf{x}_R, \mathbf{x}_S^{(i)}, t) * f_1^-(\mathbf{x}_S^{(i)}, \mathbf{x}_A, -t) * S(t), \tag{13}$$

with

$$\hat{G}^+(\mathbf{x}_A, \mathbf{x}_R, t) = \int_{\mathbb{S}_A} G^+(\mathbf{x}'_A, \mathbf{x}_R, t) * \Gamma^-(\mathbf{x}'_A, \mathbf{x}_A, t)\mathrm{d}\mathbf{x}'_A, \tag{14}$$

$$\hat{f}_1^+(\mathbf{x}_\mathrm{R}, \mathbf{x}_A, -t) = \int_{\mathbb{S}_A} f_1^+(\mathbf{x}_\mathrm{R}, \mathbf{x}'_A, -t) * \Gamma^-(\mathbf{x}'_A, \mathbf{x}_A, t)\mathrm{d}\mathbf{x}'_A. \quad (15)$$

Equation 13 is the discrete counterpart of the integral representation of equation 2. The PSF $\Gamma^-(\mathbf{x}'_A, \mathbf{x}_A, t)$ in equations 14 and 15 explains the blurring observed in Figure 5b. Deblurring this figure by MDD yields the result shown in Figure 7b, which accurately matches the ideal result in Figure 3a. The maximum deviation for the central trace is 4.7%. There are also some small edge effects, probably caused by the quantity Y (introduced in equation 7 as the inverse of f_1^-), which is not unconditionally stable. At far offsets, the amplitudes are somewhat underestimated due to our efforts to suppress the aforementioned edge effects.

TOWARD MARCHENKO IMAGING OF IMPERFECTLY SAMPLED DATA

The discrete representations of equations 12 and 13, with the blurred Green's functions and focusing functions defined in equations 9, 10, 14, and 15, form the basis for a modification of the Marchenko method, which accounts for the effects of imperfect source sampling. We propose an iterative scheme, building on the current Marchenko method, where in each iteration the effect of the PSF is removed by MDD (between the evaluation of the summation and the application of the time window). This requires an initial estimate of the PSF and an update in each iteration. The initial estimate of the PSF can be obtained from an estimate of the direct arrival of the transmission response and the initial focusing function. For the situation in which the sources as well as the receivers are imperfectly sampled and occupy different positions, we envisage an iterative scheme that combines the inversion of the discrete representations (to account for imperfect source sampling) with a sparse inversion method such as that proposed by Haindl et al. (2018) (to account for imperfect receiver sampling).

CONCLUSION

Current implementations of the Marchenko method do not account for imperfect sampling. We have derived discrete representations as an alternative for the integral representations that underlie the Marchenko method. These discrete representations account for the effects of imperfect source sampling (or, via reciprocity, of imperfect receiver sampling). The Green's functions and focusing functions expressed by these representations are blurred by PSFs, for which we derived explicit expressions.

The discrete representations form the basis for a modification of the Marchenko method, which accounts for the effects of the inherent imperfect sampling of seismic field data. The development of such a modified Marchenko method is subject of ongoing research.

ACKNOWLEDGMENTS

We thank C. Reinicke for his help with the numerical examples. We thank the editors and reviewers for their constructive comments, which helped to improve the paper. We acknowledge funding from the European Research Council (ERC) under the European Union's Horizon 2020 research and innovation program (grant agreement no. 742703).

DATA AND MATERIALS AVAILABILITY

Data associated with this research are available and can be obtained by contacting the corresponding author.

REFERENCES

Broggini, F., and R. Snieder, 2012, Connection of scattering principles: A visual and mathematical tour: European Journal of Physics, **33**, 593–613, doi: 10.1088/0143-0807/33/3/593.

Haindl, C. M., F. Broggini, M. Ravasi, and D.-J. van Manen, 2018, Using sparsity to improve the accuracy of Marchenko imaging given imperfect acquisition geometries: 80th Annual International Conference and Exhibition, EAGE, Extended Abstracts, Th-P9-14.

Peng, H., I. Vasconcelos, Y. Sripanich, and L. Zhang, 2019, On the effects of acquisition sampling on Marchenko-based focusing and primary estimation: 81st Annual International Conference and Exhibition, EAGE, Extended Abstracts, Th-R08-09.

Ravasi, M., 2017, Rayleigh-Marchenko redatuming for target-oriented, true-amplitude imaging: Geophysics, **82**, no. 6, S439–S452, doi: 10.1190/geo2017-0262.1.

Slob, E., K. Wapenaar, F. Broggini, and R. Snieder, 2014, Seismic reflector imaging using internal multiples with Marchenko-type equations: Geophysics, **79**, no. 2, S63–S76, doi: 10.1190/geo2013-0095.1.

Staring, M., and K. Wapenaar, 2019, Interbed demultiple using Marchenko redatuming on 3D field data of the Santos Basin: 16th International Congress of the Brazilian Geophysical Society, SBGf, Extended Abstracts, doi: 10.22564/16cisbgf2019.245.

Van der Neut, J., and K. Wapenaar, 2015, Point-spread functions for interferometric imaging: Geophysical Prospecting, **63**, 1033–1049, doi: 10.1111/1365-2478.12221.

Wapenaar, K., J. Thorbecke, J. van der Neut, F. Broggini, E. Slob, and R. Snieder, 2014, Green's function retrieval from reflection data, in absence of a receiver at the virtual source position: Journal of the Acoustical Society of America, **135**, 2847–2861, doi: 10.1121/1.4869083.

Wapenaar, K., J. van der Neut, E. Ruigrok, D. Draganov, J. Hunziker, E. Slob, J. Thorbecke, and R. Snieder, 2011, Seismic interferometry by crosscorrelation and by multidimensional deconvolution: A systematic comparison: Geophysical Journal International, **185**, 1335–1364, doi: 10.1111/j.1365-246X.2011.05007.x.